Widespread bacterial protein flavinylation in functionally distinct extracytosolic redox biochemistries

Raphaël Méheust,[1,2,3*] Shuo Huang,[4,5*] Rafael Rivera-Lugo,[6] Jillian F. Banfield,[1,2] Samuel H. Light[4,5]

[1]Department of Earth and Planetary Science, University of California, Berkeley, CA, USA;
[2]Innovative Genomics Institute, Berkeley, CA, USA;
[3]LABGeM, Génomique Métabolique, Genoscope, Institut François Jacob, CEA, Evry, France
[4]Duchossois Family Institute, University of Chicago, Chicago, IL, USA;
[5]Department of Microbiology, University of Chicago, Chicago, IL, USA;
[6]Department of Molecular and Cell Biology, University of California, Berkeley, CA, USA;

*These authors contributed equally
e-mail: samlight@uchicago.edu

Abstract
Disparate redox biochemistries that take place beyond the bounds of the prokaryotic cell cytosol must connect to membrane or cytosolic electron pools. Proteins post-translationally flavinylated by the enzyme ApbE mediate electron transfer in several characterized extracytosolic redox biochemistries but the breadth of functions of this modification remains unknown. Here we present a comprehensive bioinformatic analysis of 31,910 prokaryotic genomes that provides evidence of extracytosolic ApbEs within ~50% of bacteria and the involvement of flavinylation in numerous uncharacterized biochemistries. By mining flavinylation-associated gene clusters, we identify five protein classes responsible for transmembrane electron transfer and two domains of unknown function (DUF2271 and DUF3570) that are flavinylated by ApbE. We observe flavinylation/iron transporter gene colocalization patterns that suggest functions in iron reduction and assimilation. We find associations with characterized and uncharacterized respiratory oxidoreductases that highlight roles of flavinylation in respiratory electron transport chains. Finally, we identify interspecies gene cluster variability consistent with flavinylation/cytochrome functional redundancies and discover a class of “multi-flavinylated proteins" that may resemble multiheme cytochromes in facilitating longer distance electron transfer. These findings provide mechanistic insight into an important facet of bacterial physiology and establish flavinylation as a functionally diverse mediator of extracytosolic electron transfer.

Introduction

Essential microbial-environmental interactions take place beyond the bounds of the cytosol. In prokaryotes, extracytosolic biochemical processes can be situated at the extracytosolic side of the inner membrane, periplasm, cell wall, or surrounding environment. Within the extracytosolic space, redox biochemistries represent an important class of activities with functions in respiration, the maintenance/repair of extracytosolic proteins and the assimilation of minerals [1–3].

Extracytosolic redox processes require electron transfer pathways that connect with electron pools in the cytosol or membrane. Membrane proteins transfer electrons from donors, like reduced nicotinamide adenine dinucleotide (NADH) or quinols. On the extracytosolic side of the membrane, electron transfer between membrane and extracytosolic proteins is generally mediated by a redox-active protein, such as a cytochrome or thioredoxin-like protein. Cytochromes use redox-active hemes as cofactors and are often important for transferring electrons between membrane components and respiratory enzymes [2]. Thioredoxin-like proteins employ pairs of cysteines that cycle between redox states and are often involved in extracytosolic protein maturation and repair [3,4].

In addition to well established electron transfer mediators, an evolutionarily conserved flavin mononucleotide (FMN)-binding domain has more recently been implicated in extracytosolic electron transfer. FMN-binding domains are post-translationally flavinylated by the ApbE enzyme, which covalently links FMN to a conserved [S/T]GA[**S/T**]-like sequence motif (flavinylated amino acid in bold, see **Figure 1** for additional detail) within the FMN-binding domain [5]. Redox-active extracytosolic flavinylated FMN-binding domains have been identified within five characterized electron transfer systems -- including the cation pumping NQR and RNF complexes (**Figure 1A and 1B**), nitrous oxide and organohalide respiratory complexes (**Figure 1C and 1D**), and a Gram-positive extracellular electron transfer system (**Figure 1E**) [6–10]. In addition, ApbE-flavinylated motifs in homologous extracytosolic fumarate and urocanate reductases facilitate transfer from respiratory electron transport chains [11–13].

In recent years, large-scale comparative genomic analyses have emerged as a powerful tool for discovering functionally and/or mechanistically related features of prokaryotic biology [14–16]. Here, we develop a “guilt by association” approach [17] (summarized in **Supplementary Figure 1**) that exploits genomic diversity to contextualize the significance of extracytosolic flavinylation. Our analysis of *apbE*-associated gene clusters provides evidence of widespread flavinylation throughout bacteria and uncovers new connections to respiration and iron assimilation. We further identify uncharacterized aspects of extracytosolic flavinylation, including novel ApbE substrates and a class of multi-flavinylated proteins. These findings place flavinylated proteins alongside cytochromes and thioredoxin-like proteins as central mediators of bacterial extracytosolic electron transfer.

Results

Evidence of widespread extracytosolic flavinylation within bacteria

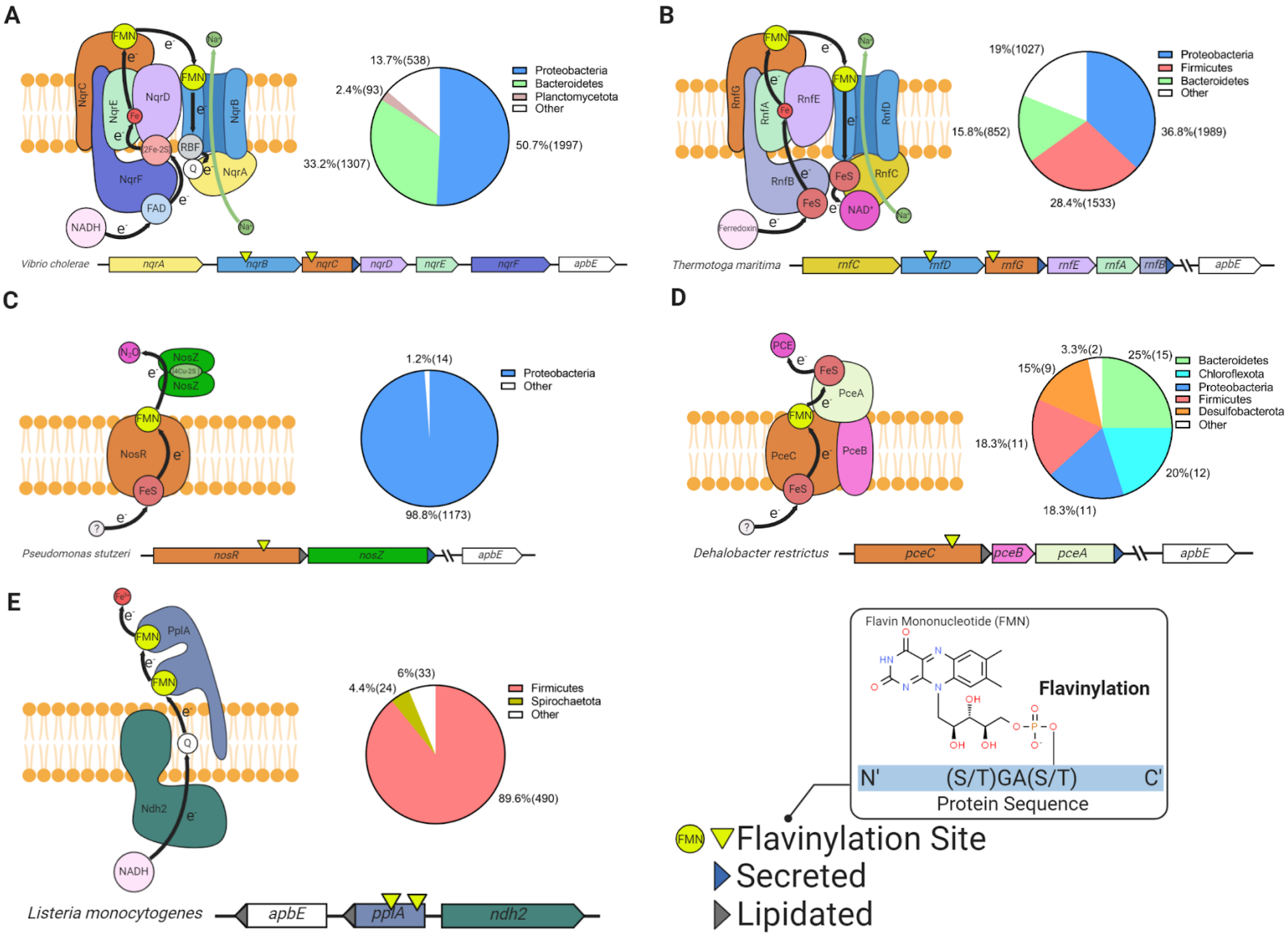

Figure 1. Characterized extracytosolic electron transfer systems with an ApbE flavinylated subunit. Representative gene clusters and models of the electron transfer complexes they encode: (A) NQR, (B) RNF, (C) nitrous oxide reduction, (D) organohalide reduction, and (E) extracellular electron transfer. Black arrows trace proposed electron transfer pathways. Accompanying pie charts show the number of genomes within each phylum that encode the electron transfer system. “Secreted” and “lipidated” refers to the presence of computationally predicted signal peptides and lipidation sites, respectively.

As all previously characterized flavinylation systems contain genes that encode for an ApbE enzyme and an FMN-binding domain-containing substrate, we reasoned that these features are indicative of flavinylation-mediated electron transfer. To identify flavinylation-mediated electron transfer systems, we searched for genes with ApbE (Pfam accession PF02424) or FMN-binding domains (Pfam accession PF04205) within a collection of 31,910 genomes that are representative of the genetic diversity of the prokaryotes [18,19]. We found that 18,965 of bacterial genomes and 238 of archaeal genomes encode an FMN binding domain-containing protein and/or an ApbE enzyme. To focus the search on extracytosolic electron transfer, we eliminated genes that lacked a computationally predicted signal peptide or lipidation site. This analysis provides evidence that ~50% of the bacterial (15,095) and ~4% of archaeal (63) genomes possess extracytosolic flavinylation components (**Supplementary Dataset**). A phylogenetic analysis of the resulting dataset reveals that extracytosolic flavinylation components are broadly distributed across bacterial life -- though strikingly underrepresented in Cyanobacteria and the Candidate Phyla Radiation (**Figure 2**).

We next took advantage of the colocalization of genes for each of the characterized systems on the genome to determine the prevalence and phylogenetic distribution of previously characterized flavinylated systems. We devised operational definitions in which the close proximity of a key gene in each system to an FMN-binding- or ApbE-containing gene was used to assign clusters to characterized systems (**Supplementary Table 1**). These analyses revealed characterized systems in 8,928 genomes broadly distributed across bacterial life (**Figure 2**).

In addition to assigning extracytosolic electron transfer functions, our analyses identified 6,230 genomes that contained evidence of extracytosolic flavinylation, but lacked a characterized extracytosolic electron transfer system. We also found that many genomes have multiple ApbE and/or FMN-binding genes and thus likely possess multiple extracytosolic electron transfer functions (**Supplementary Figure 2**). As these observations suggested that a significant proportion of extracytosolic electron transfer systems remain uncharacterized, we next turned to the identification of uncategorized flavinylation-associated gene clusters.

Domains of unknown function DUF2271 and DUF3570 are ApbE substrates

Our initial approach only considered FMN-binding domains as potential flavinylation substrates. However, preliminary analyses identified 17% of genomes (2,571 total) within our dataset that encoded an ApbE but no FMN-binding domain-containing protein – implying that some ApbE substrates lack an FMN-binding domain (**Supplementary Figure 3**). To identify novel ApbE protein substrates, we examined the genomic context of these “orphan” *apbE* genes, looking for gene cluster patterns conserved across multiple genomes (**Supplementary Dataset**).

We observed that a subset of orphan *apbE* genes are associated with DUF2271 -- a ~135 amino acid domain of unknown function. In some genomes a single gene encodes a protein with both ApbE and DUF2271 domains (e.g., NCBI Accession: RUL87804.1), but more commonly a separate DUF2271 gene

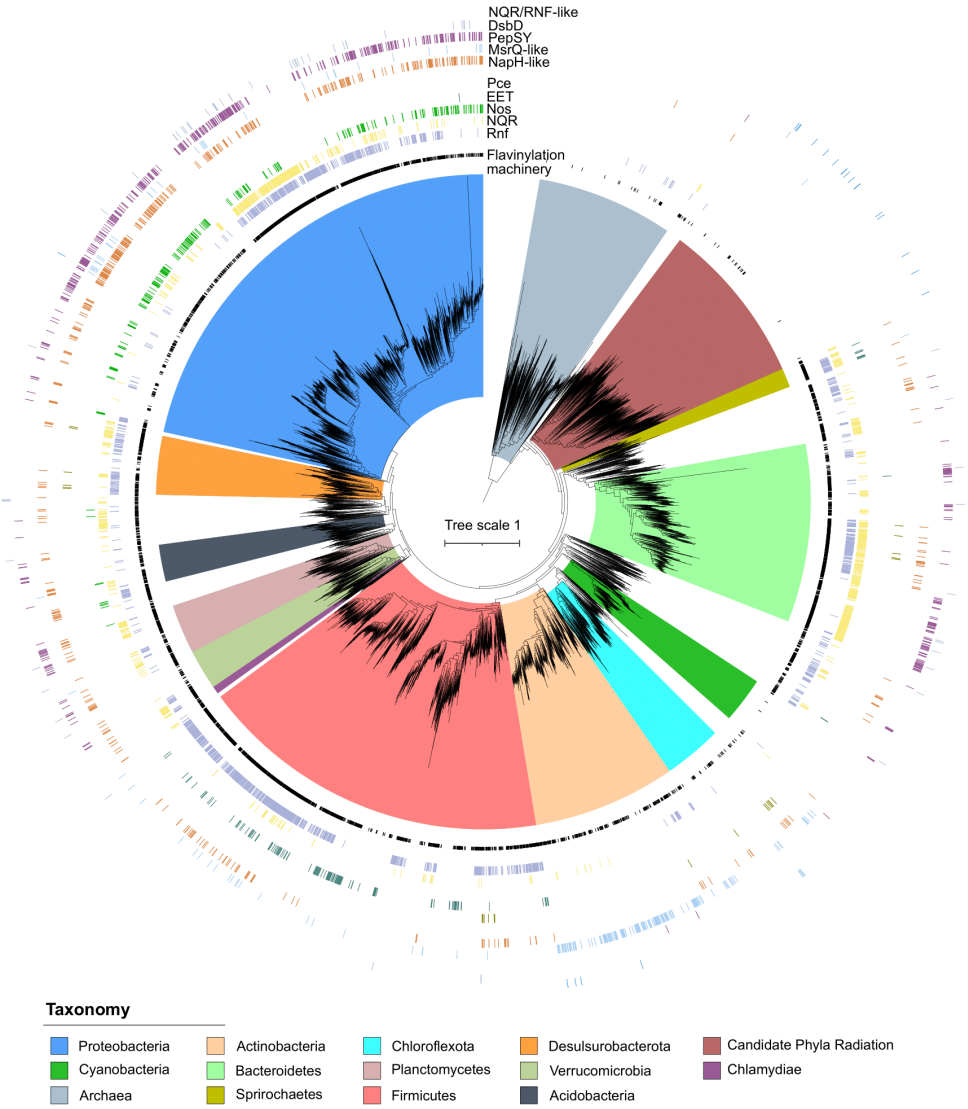

Figure 2. Phylogenetic distribution of extracytosolic protein flavinylation in prokaryotes. Phylogenetic reconstruction of the evolutionary history of 9,152 genomes representing 97% of the diversity available at the genus level in the GTDB database (9,428 distinct genera) [18]. The maximum likelihood tree was constructed based on a concatenated alignment of 14 ribosomal proteins under an LG+I+G4 model of evolution (2,850 amino-acid sites). The inner to outer rings display the presence in one genome of the genus of extracytosolic flavinylated proteins (i.e. genomes encoding a signal peptide-containing FMN-binding or ApbE) (flavinylation machinery), the presence of an RNF system, a NQR system, a Nos system, an EET system and an organohalide reduction system (Pce), the presence of a NapH-like system, a MsrQ-like system, a PepSY system, a DsbD system and a NQR/RNF-like system. The scale bar indicates the mean number of substitutions per site.

is part of a gene cluster that includes an *apbE*. Consistent with DUF2271 serving as a flavinylation substrate, we identified a conserved [S/T]GA[S/T] motif within ApbE-associated DUF2271s (**Figure 3A**). We expressed the *Amantichitinum ursilacus* DUF2271 protein in *E. coli* and found that it was flavinylated in the presence of its cognate ApbE (**Figure 3B**). Consistent with the conserved [S/T]GA[S/T] motif representing the sole ApbE target, we found that a threonine to alanine mutation at the predicted flavinylation site abrogated flavinylation (**Figure 3B**).

We observed another subset of orphan *apbE* genes that are part of gene clusters that contain a gene annotated as DUF3570 -- a ~420 amino acid domain of unknown function. Consistent with DUF3570 serving as a flavinylation substrate, we identified two conserved [S/T]GA[S/T] motifs within ApbE-associated DUF3570s (**Figure 3C**). Using the coexpression approach described above, we confirmed that the *Chlorobium luteolum* DUF3570 was flavinylated in the presence of its cognate ApbE (**Figure 3D**). Consistent with both of the identified [S/T]GA[S/T] motifs being modified, we found that serine to alanine mutations at both predicted flavinylation sites were required to abrogate flavinylation (**Figure 3D**).

We thus conclude that DUF2271 and DUF3570 are novel ApbE substrates. Including DUF2271 and DUF3570 significantly expands the number and diversity of predicted ApbE substrates and decreases the number of orphan *apbE* genomes within our dataset from 17% to 4% (670 total) (**Supplementary Figure 3**). Subsequent analyses thus likely account for a significant fraction of flavinylation substrates -- though the fact that orphan *apbE* genomes remain suggests that less prevalent ApbE substrates remain unidentified.

Identification of flavinylation-associated transmembrane electron transfer components

We next sought to gain insight into novel roles of protein flavinylation. Characterized flavinylation-based electron transfer systems are minimally defined by a cytosolic electron donor, a transmembrane electron transfer apparatus, and the flavinylated extracytosolic electron acceptor – though, in principle, the direction of electron flow could be reversed. We reasoned that identification of cytosolic and membrane components was important for understanding the extracytosolic capability of uncharacterized flavinylated systems.

To clarify the role of flavinylation-associated gene clusters, we analyzed the genomic context of a subset of representative genes with DUF3570, DUF2271, FMN-binding domain, and ApbE domains that were not assigned to a characterized system in our initial analyses. Annotations for the five upstream and five downstream genes were manually reviewed. From these gene clusters, we identified five putative transmembrane electron transfer apparatuses that are present in 6,366 genomes (**Figure 4**, **Supplementary Figure 4 and Supplementary Table 1**). The following subsections describe the organization and likely functions of these systems. Annotations of the gene clusters associated with the flavinylated systems are provided in the **Supplementary Dataset**.

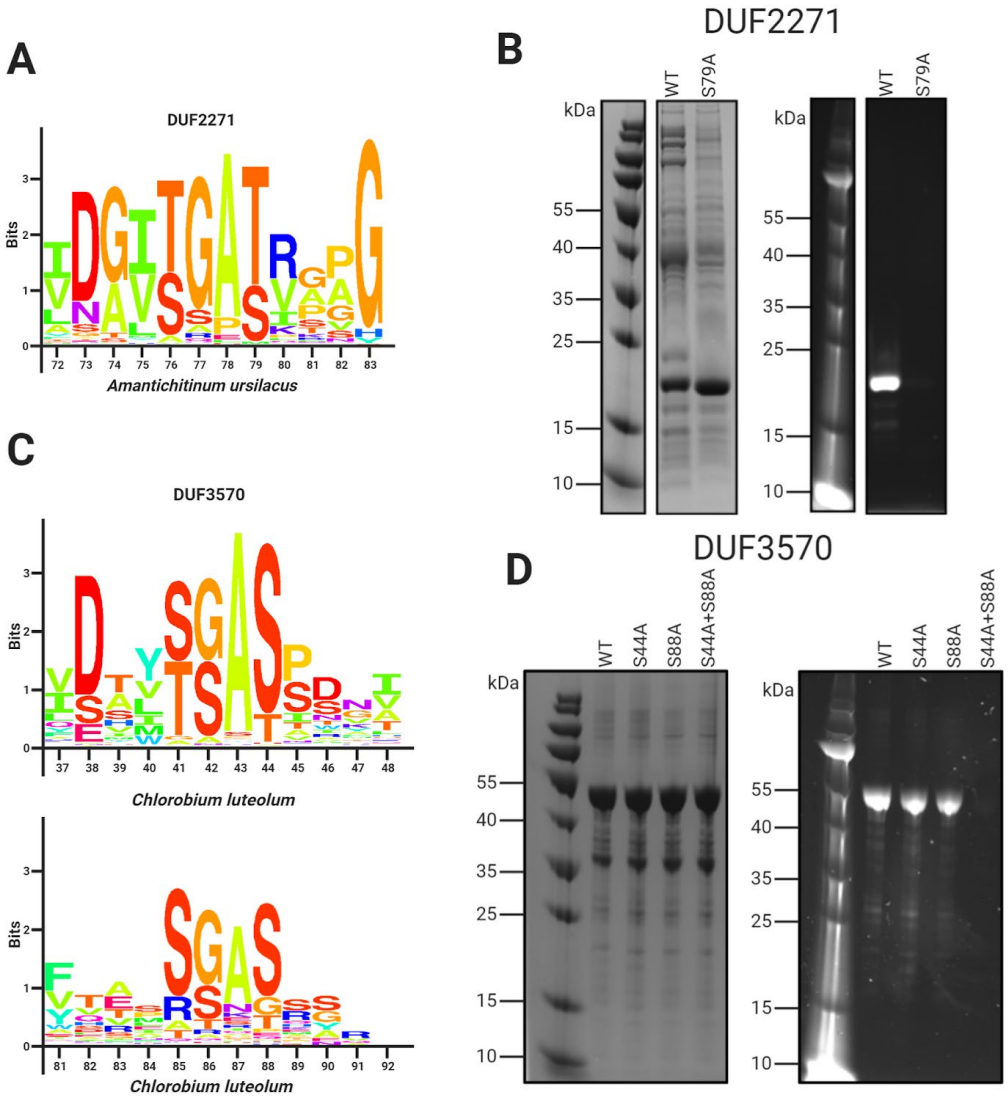

Figure 3. Domains of unknown function DUF2271 and DUF3570 are flavinylated by ApbE. (A) Conserved sequence motif within 282 flavinylation-associated DUF2271 proteins. Letter size (bits) is proportional to amino acid frequency at each position in the sequence alignment. Amino acid numbering corresponds to the *Amantichitinum ursilacus* DUF2271 sequence. (B) SDS-PAGE of purified *Amantichitinum ursilacus* DUF2271 variants coexpressed in *E. coli* with their cognate ApbE. The gel is shown with coomassie stain (left) and under ultraviolet illumination (right). (C) Conserved sequence motif within 228 flavinylation-associated DUF3570 proteins. Letter size (bits) is proportional to amino acid frequency at each position in the sequence alignment. Amino acid numbering corresponds to the *Chlorobium luteolum* DUF3570 sequence. (D) SDS-PAGE of purified *Chlorobium luteolum* DUF3570 variants coexpressed in *E. coli* with their cognate ApbE. The gel is shown with coomassie stain (left) and under ultraviolet illumination (right).

NapH-like systems

We identified 2,465 flavinylation gene clusters in 2,153 genomes that encode an "NapH-like" iron-sulfur cluster-binding protein (Pfam accession PF12801 or KEGG accession K19339) that contains several transmembrane helices (**Figure 2 and Supplementary Dataset**). These proteins are homologous to NapH, the putative quinone binding subunit of periplasmic nitrate reductase, and exhibit a broad phylogenetic distribution (**Figure 4A**) [20]. The majority of NapH-like proteins identified in our analysis contain an extracytosolic N-terminal FMN-binding domain (1,926 gene clusters) whereas the remaining ones (539 gene clusters) are in a genomic locus with a second gene that encodes an FMN-binding domain-containing protein. These proteins likely receive electrons from a donor (perhaps a quinol in some cases) that are transferred via the iron-sulfur cluster across the membrane (**Figure 4A**).

Several lines of evidence suggest that many NapH-like genes function with respiratory oxidoreductases. Previously characterized NapH-like proteins PceC and NosZ have been shown to be flavinylated and are part of gene clusters for organohalide (defined by the PceA enzyme; Pfam accession PF13486, 70 gene clusters) and nitrous oxide reduction (defined by the NosZ enzyme; KEGG accession K00376, 1,127 gene clusters), respectively (**Figure 1** and **Figure 2**) [9,10]. We also identified NapH-like gene clusters with an extracytosolic nitrite reductase (NirS, KEGG accession K15864, 133 gene clusters) and an ethanol oxidase (ExaA, KEGG accession K00114, 172 gene clusters). Thus, while the specific reactions catalyzed by the majority of NapH-like systems remains unknown, this electron transfer apparatus seems to be modularly employed to facilitate electron transfer to reductases or from oxidases (**Figure 4A**). This modularity of NapH-oxidoreductase associations is further underscored by a phylogenetic analysis, which suggests that NapH-like associations with *nirS* and *exaA* evolved independently multiple times (**Supplementary Figure 5**).

MsrQ-like systems

We identified 1,797 flavinylation gene clusters in 1468 genomes that encode an "MsrQ-like" (Pfam accession PF01794) protein **(Supplementary Dataset**). These clusters are broadly conserved in Actinobacteria and are infrequently identified in other lineages (**Figure 2 and Figure 4B)**. MsrQ-like proteins are predicted to have six transmembrane helices and two heme-binding sites. MsrQ-like proteins are homologous to MsrQ, the quinone binding subunit of periplasmic methionine sulfoxide reductase [21]. MsrQ-like proteins are also distantly related to eukaryotic proteins that function in transmembrane electron transfer, including NADPH oxidase and STEAP iron reductases [22].

MsrQ-like gene clusters typically include *apbE* and an FMN-binding domain-containing gene. MsrQ-like proteins often contain a C-terminal NAD-binding domain (Pfam accession PF00175, 1,437 gene clusters). In other cases, the MsrQ-like gene clusters include an NuoF-like protein (Pfam accession PF10589, 31 gene clusters), homologous to the NAD-binding subunit of complex I. At least a subset of MsrQ-like proteins thus likely use NAD(P)H as a cytosolic electron donor (**Figure 4B**). We also identified 153 MsrQ-like gene clusters that encode a protein homologous to the eukaryotic ferrous iron transporter

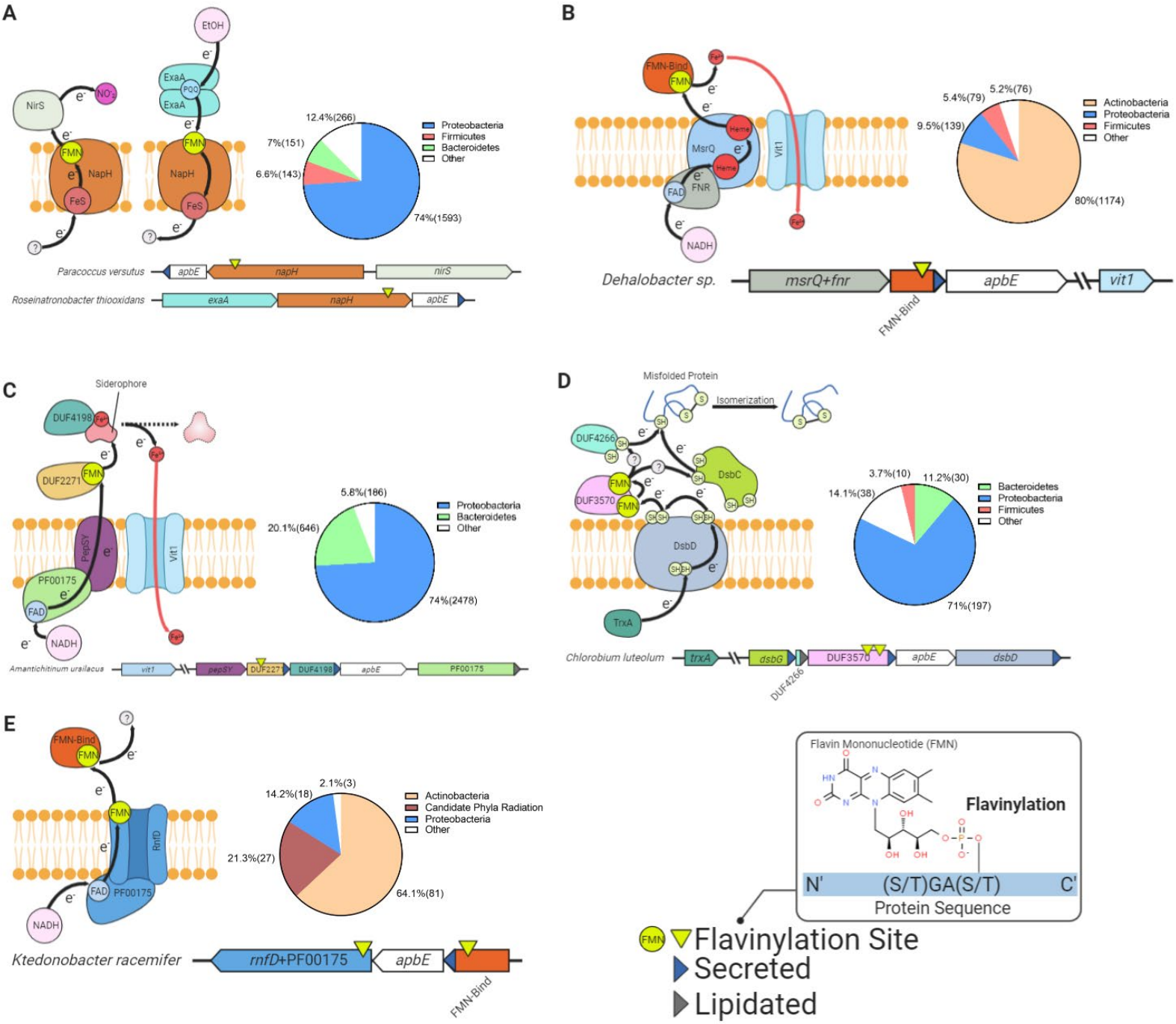

Figure 4. Uncharacterized extracytosolic electron transfer systems with an ApbE flavinylated subunit. Representative gene clusters and models of the putative electron transfer complexes they encode for: (A) NapH-like, (B) MsrQ-like, (C) PepSY, (D) DsbD, and (E) RNF/NQR-like. Black arrows trace proposed electron transfer pathways. Accompanying pie charts show the number of genomes within each phylum that encode the electron transfer system. “Secreted” and “lipidated” refers to the presence of computationally predicted signal peptides and lipidation sites, respectively.

VIT1 (PFAM accession PF01988). This association suggests that some MsrQ-like systems function as assimilatory iron reductases that facilitate iron uptake through VIT1 (**Figure 4B**).

PepSY-like systems

We identified 3,220 flavinylation gene clusters in 3,040 genomes that encode a PepSY-like (Pfam accessions PF03929 and PF16357) protein (**Supplementary Dataset**). PepSY-like proteins contain three transmembrane helices and are broadly distributed throughout Gram-negative bacteria (**Figure 2 & 4C**). PepSY-like gene clusters frequently encode an ApbE enzyme, the flavinylation substrate DUF2271 (Pfam accession PF10029, 2,833 clusters), and a secreted DUF4198 (Pfam accession PF10670, 1,500 clusters) protein. Little is known about the structure or function of PepSY-like proteins. The only characterized PepSY-like homolog, *Vibrio cholerae* VciB (which is not associated with identified flavinylation components) was reported to possess extracytosolic iron reductase activity [23]. This activity is consistent with PepSY-like proteins possessing transmembrane electron transfer activity. We further identified 1,077 PepSY-like genes that have a NAD-binding domain (Pfam accession PF00175), suggesting that a subset of these proteins use cytosolic NADH as an electron donor (**Figure 4C**).

Several observations implicate a role for identified PepSY-like gene clusters in iron reduction and assimilation. First, a functional connection to MsrQ-like proteins is suggested by our observation that 108 gene clusters contain both PepSY-like and MsrQ-like genes. Second, 167 PepSY-like gene clusters contain a VIT1 (Pfam accession PF01988) ferrous iron transporter (**Figure 4C**). Finally, PepSY-like gene clusters have been shown to be repressed by Fur (the primary transcription regulator that responds to iron limitation) in *Shewanella oneidensis* and *Caulobacter crescentus* [24,25]. Moreover, in some cases, PepSY-like proteins may be actively involved in the extraction of siderophore-bound iron, as periplasmic reduction has been shown to be important for the uptake of siderophore-bound iron and 231 PepSY-like gene clusters encode a TonB receptor (Pfam accession PF03544) related to well-characterized outer membrane siderophore transporters (**Figure 4C**) [26,27].

DsbD systems

We identified 285 flavinylation gene clusters in 275 genomes that contain a DsbD protein (Pfam accession PF02683) (**Figure 2 and Supplementary Dataset**). DsbD is part of a well-studied transmembrane protein family that uses cysteine pairs to transfer electrons across the membrane [28,29]. DsbD family proteins generally transfer electrons onto extracytosolic thioredoxin-like proteins, which in turn use a similar thiol-disulfide exchange chemistry to promote extracytosolic redox-dependent activities, such as oxidative protein folding [3].

The DsbD gene clusters identified in our analyses typically include genes for ApbE, the flavinylation substrate DUF3570 (Pfam accession PF12094, 227 clusters), a thioredoxin-like protein (Pfam accession PF13899, 183 clusters), and a DUF4266 protein (Pfam accession PF14086, 221

clusters). DUF4266 is a small secreted protein with a highly conserved C-terminal cysteine-(any amino acid)-cysteine (CXC) sequence motif that may undergo redox cycling.

We also detected 316 gene clusters that encode ApbE/DUF3570-thioredoxin-like/DUF4266, but do not colocalize on the genome with DsbD – implying that this system may be more common than is revealed by the DsbD-dependent analysis presented in **Figure 2**. These observations suggest that a hybrid thioredoxin-like/flavinylation-based system receives electrons from DsbD in some bacteria (**Figure 4D**). While the function of DUF3570-based electron transfer remains uncertain, 25 gene clusters contain a VIT1 ferrous iron transporter and thus may play a role in iron assimilation (**Supplementary Dataset**).

NQR/RNF-like systems

We identified 127 flavinylation gene clusters in 127 genomes, primarily within Actinobacteria and the Candidate Phyla Radiation genomes, with evidence of partial NQR or RNF systems (**Figure 2**). As shown in **Figure 1**, the NQR and RNF complexes contain a common core apparatus with two transmembrane electron transfer pathways that together achieve a semicircular electron flow [30,31]. A first path takes electrons from the cytosol to the extracytosolic FMN-binding domain, while a second path takes electrons from the FMN-binding domain back to a cytosolic substrate. NQR/RNF-like gene clusters encode for components associated with a single electron transfer pathway and thus likely function for unidirectional electron flow (**Figure 4E**).

NQR/RNF-like gene clusters encode a protein with an N-terminal membrane domain that is homologous to NqrB/RnfD and a cytosolic C-terminal domain homologous to the NAD-binding domain NqrF (Pfam accession PF00175). NqrB/RnfD is flavinylated by ApbE and plays a role in electron transfer across the membrane. This system presumably uses NAD(P)H as a cytosolic electron donor for electron transfer to an extracytosolic FMN-binding domain. Six NQR/RNF-like gene clusters contain a VIT1 ferrous iron transporter, suggesting that some of these systems function in iron assimilation (**Supplementary Dataset**).

Other flavinylated proteins implicated in iron assimilation and respiration

We next asked about the function of flavinylation-associated gene clusters that lack a core transmembrane electron transfer system. This category of extracytosolic proteins presumably rely on proteins encoded elsewhere on the genome to link up with membrane electron pools. Inspection of these gene clusters led to the identification of two noteworthy examples that are described in the following subsections.

P19-associated iron assimilation

A gene cluster that includes the ferrous iron binding protein P19 (Pfam accession PF10634) and the FTR1 (Pfam accession PF03239) iron transporter has previously been shown to encode a mechanistically uncharacterized system involved in iron assimilation [32]. We identified 260 P19 gene

clusters, mostly in Gram-positive bacteria, that contain a gene with an FMN-binding domain (**Supplementary Figure 6A & 6B and Supplementary Dataset**). Interestingly, many Gram-negative P19 gene clusters lack an FMN-binding gene, but contain an additional thioredoxin-like gene [33] (**Supplementary Figure 6B**). The role of the FMN-binding/thioredoxin-like protein in these systems has not been defined, but, similar to other assimilatory iron reductases, could engage in redox chemistry to facilitate iron uptake. These observations thus establish another connection between flavinylation and microbial iron assimilation and highlight functional parallels between flavinylation and thioredoxin-like extracytosolic electron transfer.

Fumarate reductase-like oxidoreductases

Fumarate reductase-like enzymes (members of the Pfam accession PF00890 enzyme superfamily) are a group of evolutionarily related proteins that catalyze a variety of redox reactions -- though phylogenetic analyses suggest that substrates for many members of the superfamily remain unknown [11,34]. We observe that fumarate reductase-like enzymes often contain an FMN-binding domain (3,070 proteins encoded by 2,979 distinct gene clusters in 1,236 genomes) or are part of gene clusters (+/- 2 genes) that contain an FMN-binding domain (189 gene clusters in 171 genomes) (**Supplementary Dataset**). Several characterized fumarate reductase-like enzymes (including fumarate, urocanate, and methacrylate reductases) are extracytosolic and function in respiration [11,12,35]. The *Listeria monocytogenes* fumarate reductase and the *S. oneidensis* urocanate reductase have been shown to be flavinylated [11,12]. In both cases, the flavinylation motif is thought to facilitate electron transfer from electron transport chain components encoded elsewhere on the genome to the enzyme active site [11,13]. These observations thus suggest that FMN-binding domains mediate electron transfer from membrane components to a prevalent class of extracytosolic reductases and highlight another connection between flavinylation and respiration.

Modular flavinylation/cytochrome usage in respiratory systems

A comparison of extracytosolic electron transfer systems identified in our analyses revealed multiple instances in which cytochrome and flavinylated electron transfer components appear to be performing similar electron transfer roles within related systems. For example, we identified a flavinylated NapH-like protein that is well situated to mediate electron transfer from the extracytosolic alcohol oxidase to the electron transport chain, where a cytochrome c protein has been shown to play this role in other microbes (**Figure 5A**) [36].

Another example of this dynamic is provided by a comparison of fumarate reductases. The extracytosolic *S. oneidensis* fumarate reductase contains an N-terminal muti-heme cytochrome c domain (Pfam accession PF14537), whereas the related *L. monocytogenes* enzyme uses an FMN-binding domain to connect to the electron transport chain (**Figure 5B**) [11,37]. Different microbes thus seem to utilize

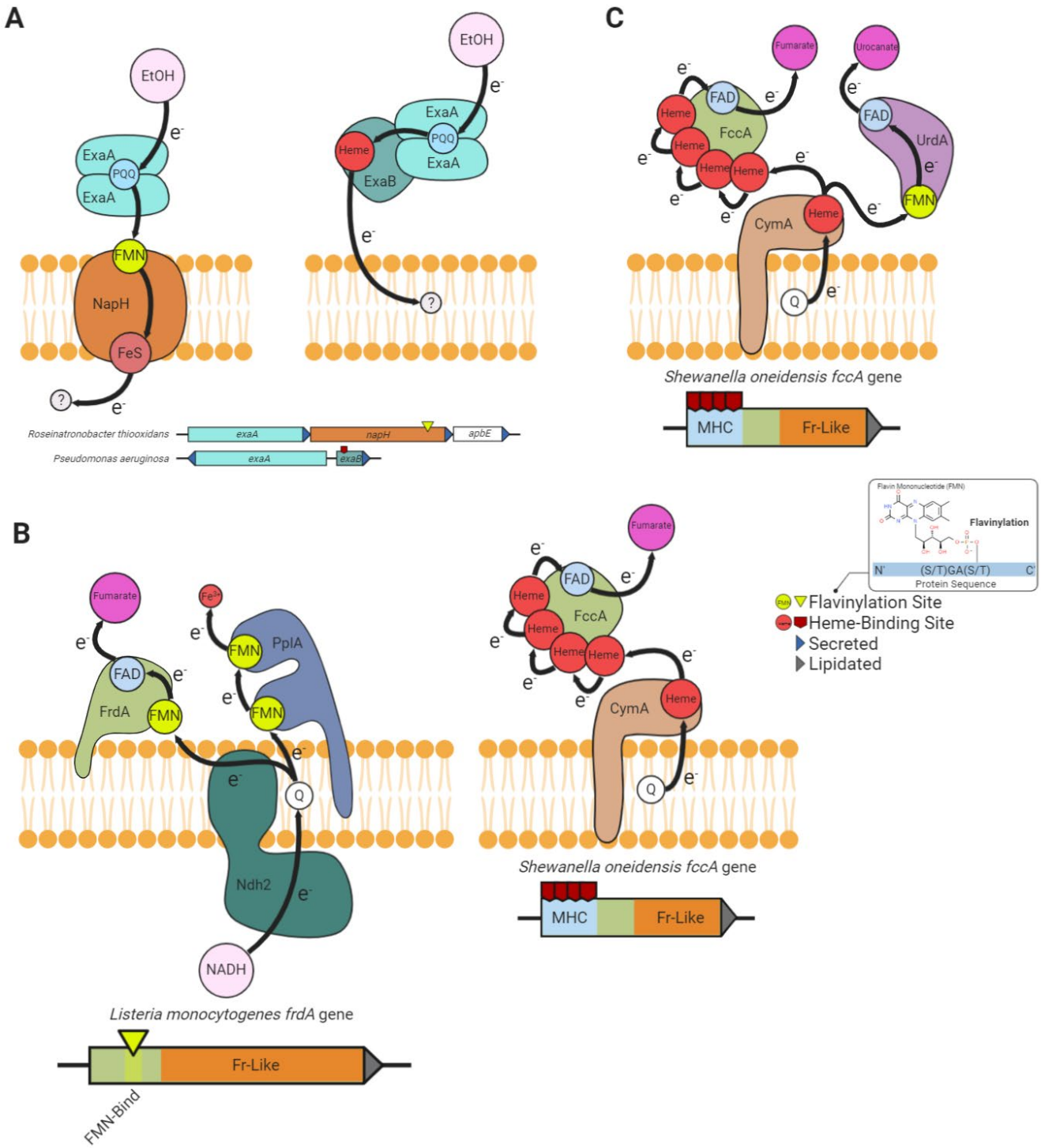

Figure 5. Modular flavinylation/cytochrome usage in extracytosolic electron transfer. (A) *Pseudomonas aeruginosa* and *R. thiooxidans exaA* alcohol oxidase gene clusters and the proposed electron transfer pathways they encode. (B) Domain structure of *L. monocytogenes* and *S. onedensis* fumarate reductases (FrdA and FccA, respectively) and proposed electron transfer mechanisms. (C) Proposed electron transfer mechanisms to *S. onedensis* fumarate reductase-like enzymes, fumarate reductase (FccA) and urocanate reductase (UrdA).

flavinylation and cytochrome domains in a similar fashion to link respiratory enzymes to electron transport chains.

We further found the type of flavinylation/cytochrome substitution observed for fumarate reductase to be indicative of a broader pattern within fumarate reductase-like enzymes. We identified 147 gene clusters within 108 genomes that encode separate fumarate reductase-like and cytochrome proteins and 879 genes within 360 genomes that encode a single protein with both fumarate reductase-like and cytochrome domains (**Supplementary Table 2**). Many genomes encode multiple fumarate reductase-like paralogs and 99 genomes encode both cytochrome- and flavinylation-associated enzymes (**Supplementary Table 2**). This dynamic is exemplified by *S. oneidensis*, which in addition to the mentioned cytochrome-associated fumarate reductase contains a flavinylated urocanate reductase that also exhibits a respiratory function (**Figure 5C**) [12]. Broadly similar flavinylation- and cytochrome-based extracytosolic electron transfer mechanisms thus seemingly coexist within some microbes.

Multi-flavinylated proteins may facilitate longer distance electron transfer

Multi-heme cytochromes are proteins that bind multiple hemes to achieve longer distance extracytosolic electron transfer [38]. Among other functions, multiheme proteins are important for transferring electrons across the cell envelope to insoluble electron acceptors that are inaccessible within the cytosolic membrane [39,40]. We have observed that extracytosolic proteins with multiple FMN-binding domains are also common (2,081 proteins in 1,530 genomes), particularly in Gram-positive bacteria, and contain as many as 13 predicted flavinylation sites **(Figure 6A & 6B and Supplementary Dataset)**. Multi-cofactor binding properties thus establish another parallel between cytochrome and flavinylation-based electron transfer.

Gene cluster analyses provide some insight into the basis of multi-flavinylated protein electron transfer. We find that multi-flavinylated proteins are often associated with established transmembrane electron transfer components and thus likely receive electrons through conventional mechanisms (**Figure 6C**). We observe that some clusters contain large unannotated proteins with putative cell wall-binding domains -- such as SLH (Pfam accession PF00395), Rib (Pfam accession PF08428), FIVAR (Pfam accession PF07554), or LysM (Pfam accession PF01476) -- and are thus likely involved in redox biochemistries at the cell wall or at the cell surface (**Figure 6D**). We also identified 157 clusters that encode a multi-flavinylated protein and up to 4 additional proteins with FMN-binding domains (**Figure 6D & 6E**). These observations suggest that some multi-flavinylated proteins are part of multi-step electron transfer pathways and may form elaborate multi-protein complexes that span the cell wall.

The role of multi-flavinylated gene clusters is generally unclear, with only a minority of clusters providing limited functional clues. We identified a subset of clusters that encode proteins with multiple fumarate reductase-like domains that likely establish an unusual multi-functional reductase platform (**Figure 6D & 6G**). We also identified a number of RNF clusters that contain multi-flavinylated RnfGs (the extracytosolic flavinylated subunit in RNF complexes) (**Figure 6C**). These multi-flavinylated RNF

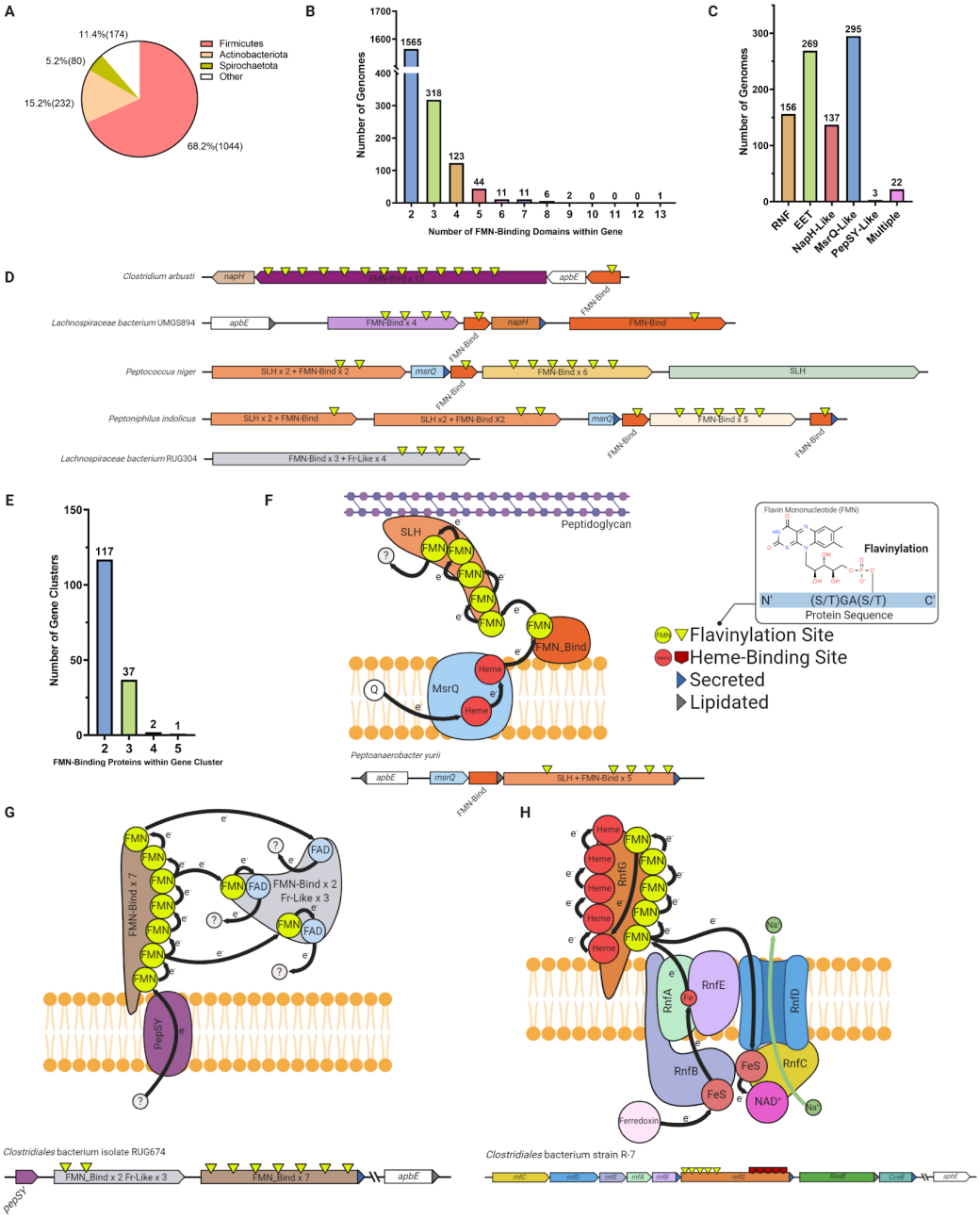

Figure 6. Multi-flavinylated proteins may possess novel electron transfer properties. (A) Pie chart showing the number of genomes within each phylum that contain a multi-flavinylated (i.e., >1 FMN-binding domain) protein. (B) Histogram showing the number of FMN-binding domains within identified multi-flavinylated proteins. (C) Histogram showing the number of multi-flavinylated protein gene clusters that encode one of the transmembrane electron transfer systems described in **Figures 1 and 4**. (D) Examples of multi-flavinylated protein gene clusters. Fumarate reductase-like domains are abbreviated as Fr-like. (E) Histogram showing the number of encoded proteins containing at least one FMN-binding domain within multi-flavinylated protein gene clusters. (F) Model of a possible electron transfer path encoded by a representative multi-flavinylated gene cluster that includes a protein with a cell wall-binding domain. (G) Model of a possible electron transfer path encoded by a representative multi-flavinylated gene cluster that includes multiple Fr-like domains. (H) Model of possible bifurcated electron transfer pathway encoded by a RNF complex with a multi-flavinylated/multi-heme cytochrome RnfG.

complexes likely provide a second electron transfer pathway that facilitates transfer to alternative extracytosolic acceptors. This type of bifurcated electron transfer would be similar to a multi-heme cytochrome-based transfer mechanism recently suggested in studies of a methanogen RNF [41]. Interestingly, we also identified a subset of multi-flavinylated RnfGs in the family Christensenellales that contain a multi-heme cytochrome domain and thus may assume additional functions relevant for cytochrome-based electron transfer (**Figure 6H**). While much remains to be learned, preliminary observations are thus consistent with multi-flavinylated proteins establishing functionally diverse complex electron transfer pathways.

Discussion

Comparative analysis of gene clusters within large collections of prokaryotic genomes has emerged as a powerful discovery tool in recent years. Our large-scale survey of diverse genomes extends this approach and suggests that ApbE-mediated extracytosolic flavinylation is a prominent feature of bacterial physiology. More granular analyses of gene clusters provide evidence consistent with flavinylation usage in diverse redox biochemistries and considerable insight into specific functionalities. Collectively, these studies suggest that flavinylation represents a major component of microbial extracytosolic electron transfer -- in part because modular usage facilitates its involvement in various biochemical processes.

Previous studies of prokaryotic extracytosolic electron transfer have largely focused on cytochromes and thioredoxins. Flavinylated systems exhibit both similarities to and distinctions from these systems -- with the parallels to cytochrome-based electron transfer being particularly noteworthy. The apparent functional interchangeability in the electron transfer capabilities of iron- and flavin-containing proteins is reminiscent of the relationship between ferredoxins and flavodoxins. Ferredoxins and flavodoxins are redox-active proteins that function in a number of cytosolic biochemistries and contain iron and flavin cofactors, respectively [42]. Microbes switch from ferredoxin to flavodoxin usage in iron-poor environments – presumably because minimizing the demand for iron cofactors is important for conserving the cellular iron reserve in this context [43,44]. Based on this precedent, it seems plausible that flavinylation-based electron transfer mechanisms might be particularly advantageous within iron-poor environments. The co-existence of functionally similar but mechanistically distinctive flavinylation- and cytochrome electron transfer components may thus reflect divergent resource management strategies across distinct environments.

Of the proteins linked to extracytosolic electron transfer by our studies, the class of multi-flavinylated proteins are particularly intriguing. These proteins may resemble multi-heme cytochromes in their use of multiple redox-active cofactors to achieve longer distance electron transfer. A particularly noteworthy aspect of multi-heme cytochromes concerns their ability to establish “nanowires” that have a variety of potential biotechnological applications [38,45]. In contrast to one-electron transferring hemes,

flavins possess two-electron transferring properties [46]. The electron transferring behavior of multi-flavinylated proteins thus represents an interesting subject for future studies and may have implications for the development of redox-based biotechnologies.

Materials and Methods

Genome collection

The 30,238 bacterial and 1,672 archaeal genomes from the GTDB database (release 05-RS95 of 17th July 2020) were downloaded with the taxonomy and the predicted protein sequences of the genomes [18].

Functional annotation

Protein sequences were functionally annotated based on the accession of their best Hmmsearch match (version 3.3) (E-value cut-off 0.001) [47] against the KOfam database (downloaded on 02-18-2020) [48]. Domains were predicted using the same Hmmsearch procedure against the Pfam database (version 33.0) [49]. SIGNALP (version 5.0) was run to predict the putative cellular localization of the proteins using the parameters -org arch in archaeal genomes and -org gram+ in bacterial genomes [50]. Prediction of transmembrane helices in proteins was performed using TMHMM (version 2.0) (default parameters) [51].

Identification of flavinylated systems

The five genes downstream and upstream of an ApbE, FMN-binding domain, DUF3570 or DUF2271 encoding genes were first collected. Only gene clusters with at least one signal peptide or lipidation site predicted in one of the four target genes were considered for further analysis and were referred to as flavinylation-associated gene clusters. The flavinylation-associated gene clusters were then assigned to a flavinylated system based on the presence of key genes reported in the **Supplemental Table S1**.

Phylogenetic analyses of the “NapH-like” iron-sulfur cluster-binding protein sequences

The “NapH-like” iron-sulfur cluster-binding protein tree was built as follows. Sequences were aligned using MAFFT (version 7.390) (–auto option) [52]. The alignment was further trimmed using Trimal (version 1.4.22) (–gappyout option) [53]. Tree reconstruction was performed using IQ-TREE (version 1.6.12) [54], using ModelFinder to select the best model of evolution [55], and with 1000 ultrafast bootstrap [56].

Concatenated 16 ribosomal proteins phylogeny

A maximum-likelihood tree was calculated based on the concatenation of 14 ribosomal proteins (L2, L3, L4, L5, L6, L14, L15, L18, L22, L24, S3, S8, S17, and S19). Homologous protein sequences were aligned using MAFFT (version 7.390) (--auto option) [52] and alignments refined to remove gapped regions using Trimal (version 1.4.22) (--gappyout 570 option) [53]. The protein alignments were concatenated with a final alignment of 9,152 genomes and 2,850 positions. Tree reconstruction was performed using IQ-TREE

(version 1.6.12) [54]. A LG+I+G4 model of evolution was selected using ModelFinder [55] and 1000 ultrafast bootstraps were performed [56].

DUF2271 and DUF3570 sequence analyses

Sequences of flavinylation-associated DUF3570 and DUF2271 proteins were aligned using EMBL-EBI Clustal Omega Multiple Sequence Alignment [57]. Sequence logos of the flavinylation sites shown in **Figure 3** were generated in R using the "ggseqlogo" package [58].

DUF2271 and DUF3570 overexpression and purification

A synthetic construct of the signal peptide-truncated *Amantichitinum ursilacus* IGB-41 DUF2271 gene (NCBI accession: WP_053936890.1) was subcloned into the pMCSG53 vector. A second construct contained a ribosome-binding site and the signal peptide-truncated cognate *apbE* (NCBI accession: WP_053936888.1) just downstream of the DUF2271 gene. A similar cloning strategy was used for the *Chlorobium luteolum* DSM 273 DUF3570 (NCBI accession: ABB24424.1) and its cognate *apbE* (NCBI accession: ABB24423.1). Point mutations of DUF3570 and DUF2271 were generated using the NEB Q5® Site-Directed Mutagenesis Kit. Briefly, overlapping primers containing mutated sequences were used in a PCR reaction using pMCSG53::DUF3570 or pMCSG53::DUF2771 as DNA template to generate expression vectors containing respective mutant sequences. Plasmids containing wild-type protein sequences were removed using digestion with the DpnI enzyme, which only acts on methylated DNA sequences.

Sequence verified plasmids were transformed in *E. coli* BL21 cells (Rosetta DE3, Novagen). A single colony of each expression strain was isolated on Luria-Bertani (LB) agar supplemented with carbenicillin (100ug/mL) and inoculated into 15 mL of LB. Following overnight growth, cultures were diluted in 500 mL of Brain heart infusion (BHI) broth to a final OD600 of 0.1. When the OD600 reached 0.7 to 1 protein overexpression was induced by adding Isopropyl β-d-1-thiogalactopyranoside (IPTG) to a final concentration of 1 mM. The culture was then incubated overnight at 25°C with aeration and collected by centrifugation (7,000 x g for 15 min). After removing the supernatant, cells were washed in 30 mL of lysis buffer (5:1 v/weight of pellet; 300 mM NaCl, 1 mM Dithiothreitol (DTT), 10 mM imidazole, 1 mM Ethylenediaminetetraacetic acid (EDTA), and 50mM Tris-HCl pH = 7.5). Pelleted cells were stored at -80°C overnight, resuspended in lysis buffer, lysed by sonication (8 x 30 second pulses), and cleared by centrifugation (40,000 x g for 30 min).

For the purification of *A. ursilacus* DUF2271, cell lysate was collected and loaded onto a 5mL HisTrapTM column (GE Healthcare) using the ÄKTA Pure FPLC. Protein was eluted using an imidazole concentration gradient with a maximal concentration of 500 mM. Protein concentrations of eluted fractions containing His_6-tagged DUF2271 were measured on a DeNovix DS-11 FX+ Spectrophotometer based on protein molar mass and extinction coefficient and standardized to 0.4 mg/mL.

Initial observations revealed that the majority of expressed *C. luteolum* DUF3570 was present in the lysed cell pellet. To purify *C. luteolum* DUF3570, the cell pellet was washed with wash buffer (10:1 v/weight of pellet; 100 mM Tris-HCl pH = 7.5, 300 mM NaCl, 2 mM 2-mercaptoethanol, 1 M guanidine-HCl, 1 mM EDTA, and 2% w/v TritonTM X-100) and centrifuged at 40,000 x g for 30 min. The supernatant was then discarded and this washing step was repeated until the supernatant was clear. The cell pellet was then resuspended in wash buffer (10:1 v/weight of pellet) without guanidine-HCl and TritonTM X-100 and centrifuged (40,000 x g for 15 min) to remove guanidine-HCl and TritonTM X-100. After supernatant was discarded, the pellet was resuspended in extraction buffer (4:1 v/weight of pellet; 100 mM Tris-HCl pH = 7.5, 300 mM NaCl, 10 mM imidazole, 6 M guanidine-HCl, 2 mM 2-mercaptoethanol, and 1 mM EDTA) and protein was denatured by overnight rotator mixation. Supernatant containing denatured DUF3570 was collected by centrifugation (20,000 x g for 30 min).

Subsequent *C. luteolum* DUF3570 purification steps were conducted on a Ni-NTA column. Specifically, 4 mL of Ni-NTA slurry (NuviaTM IMAC Resin, 25 mL) were added into a glass chromatography column (Econo-Column®, 1.0 x 10 cm). The column was prepared with 10 mL of column wash buffer and the samples containing denatured DUF3570 were then loaded. Bound protein was eluted using 5 mL of modified column wash buffer containing 50, 100, 200, or 500 mM of imidazole. To prevent guanidine-HCl from forming precipitates with SDS in following steps, eluted samples were mixed with 100% ethanol (9:1 v/v) and incubated at -20°C for 10min. After centrifugation at 21,100 x g for 5 min and removal of the supernatant, the pelleted protein was washed once with 90% ethanol. The sample was centrifuged again and the pellet was resuspended in diH_2O. Protein concentrations of eluted fractions containing His_6-tagged DUF3570 were measured as described above and standardized to 1.2 mg/mL.

DUF2271 and DUF3570 flavinylation analyses

Purified and normalized DUF2271 and DUF3570 were loaded and separated on a 12% Bis-Tris gel. Prior to gel staining, flavinylated bands were visualized under UV due to the UV resonance of the flavin molecule. Visualizations of Coomassie blue stained protein were captured with an iBright 1500 gel imager.

Acknowledgements

We thank Daniel Portnoy and Dominique Missiakas for providing critical feedback on the manuscript. R.M. and J.F.B. acknowledge funding support from the Chan Zuckerberg Biohub and the Innovative Genomics Institute at University of California, Berkeley. R.R-L acknowledges funding support from The National Academies of Sciences, Engineering, and Medicine (Ford Foundation Fellowship). S.H.L. acknowledges funding support from the National Institute of Allergy and Infectious Diseases of the National Institutes of Health (K22 AI144031).

Supplementary Dataset. Gene clusters of the ten flavinylated systems discussed in this study (RNF, NQR, Nos, extracellular electron transfer, organohalide respiration, NapH-like, MsrQ-like, NQR/RNF-like, DsbD/DsbD-like, and PepSY-like), the P19 system, DUF2271, DUF3570, and multiflavinylated proteins. The five genes downstream and upstream of each key gene (column K) were identified and annotated using signal peptide prediction (column G), transmembrane helix prediction (column H), PFAM (column I) and KEGG databases (column J). Genome accession and taxonomy are presented in columns A and B, respectively. Open reading frame (ORF) accessions are shown in column C. Columns D and E correspond to the scaffold accession and the ORF coordinates on the scaffold (start, end, and strand). Column F indicates the size of ORFs in amino acids.

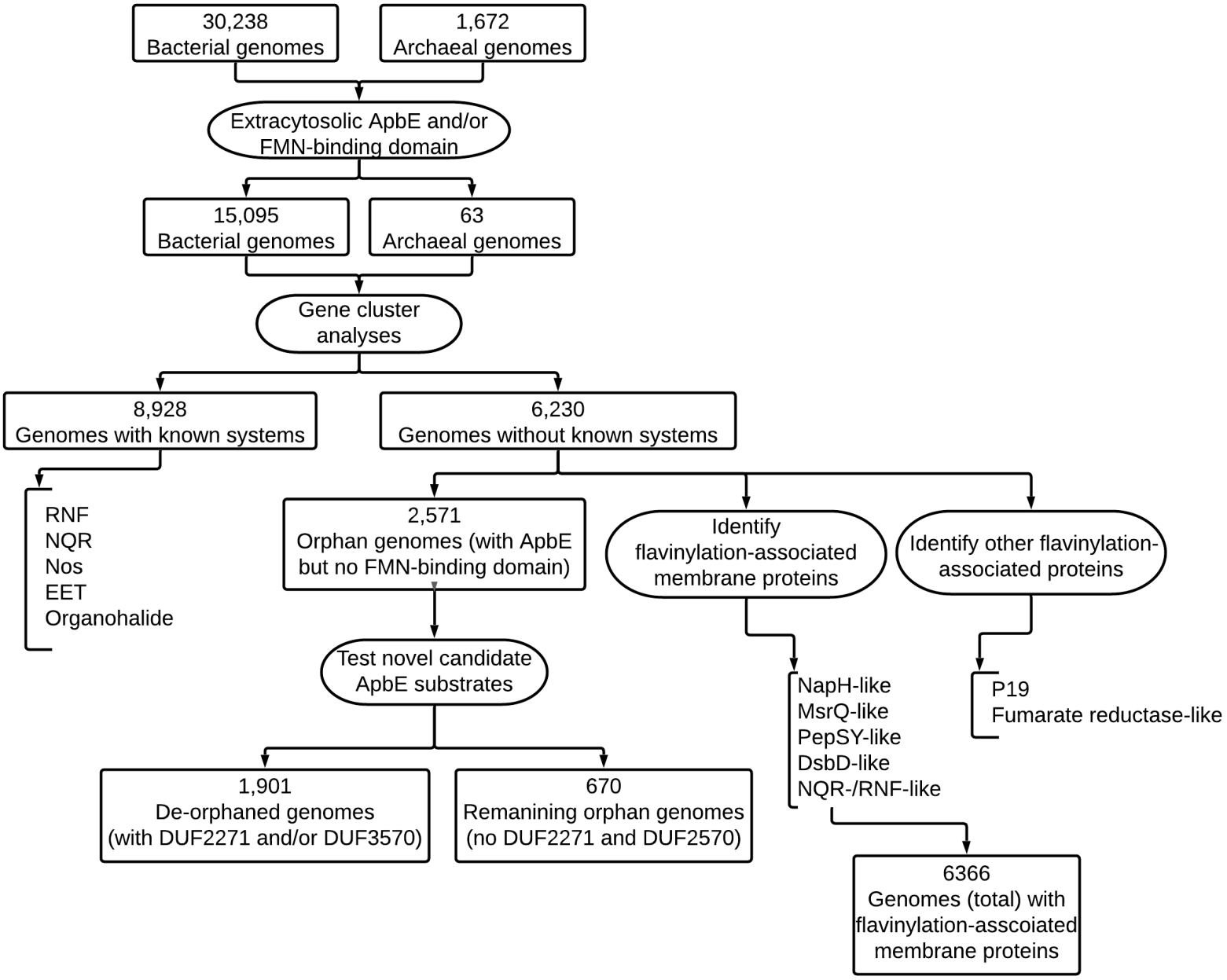

Supplementary Figure 1. Summary of the discovery strategy followed by described studies.

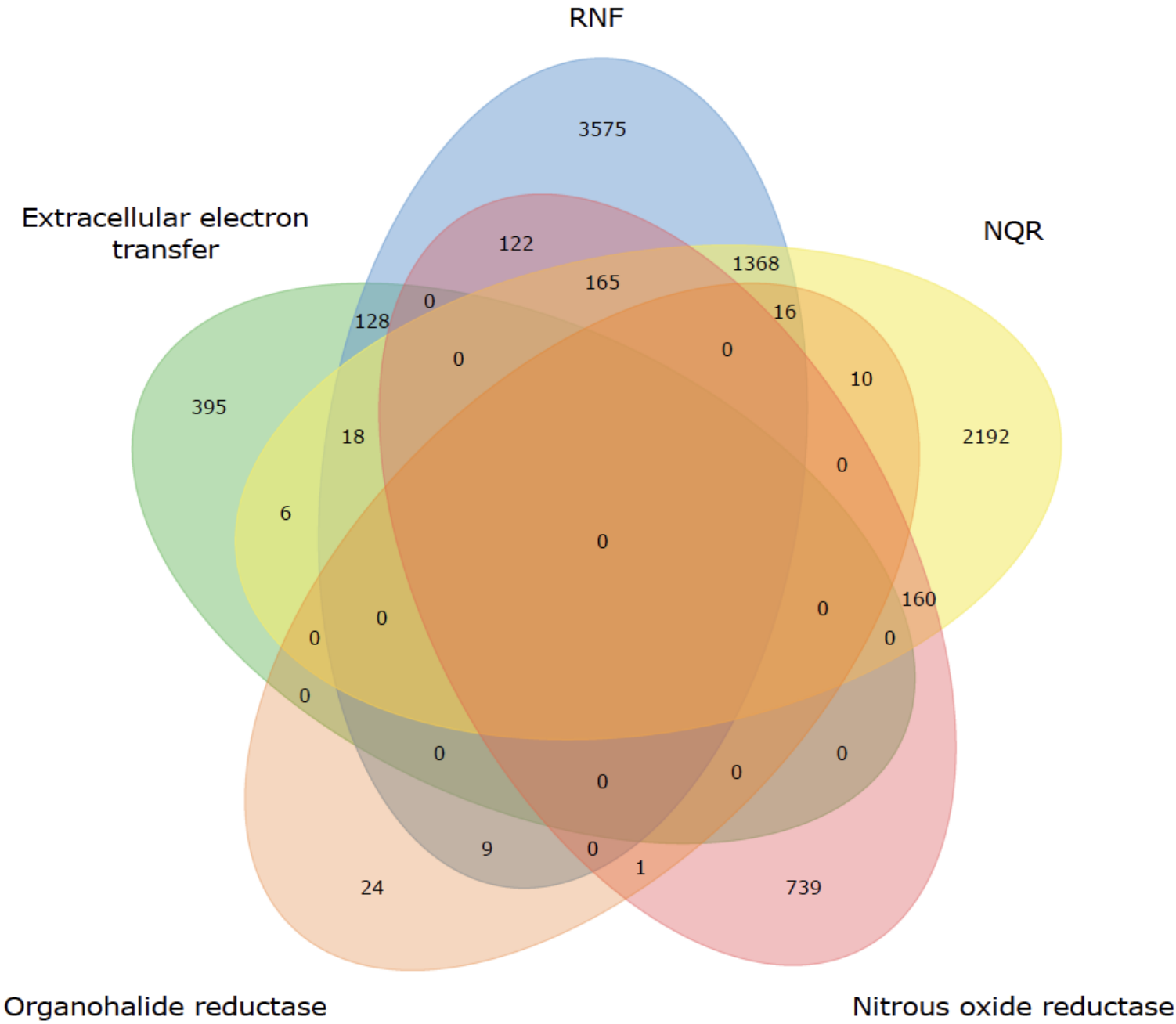

Supplementary Figure 2. Distribution of characterized extracytosolic electron transfer systems within prokaryotic genomes. Venn diagram showing the number of characterized systems within the 8,928 genomes that have at least one of the previously characterized extracytosolic electron transfer systems.

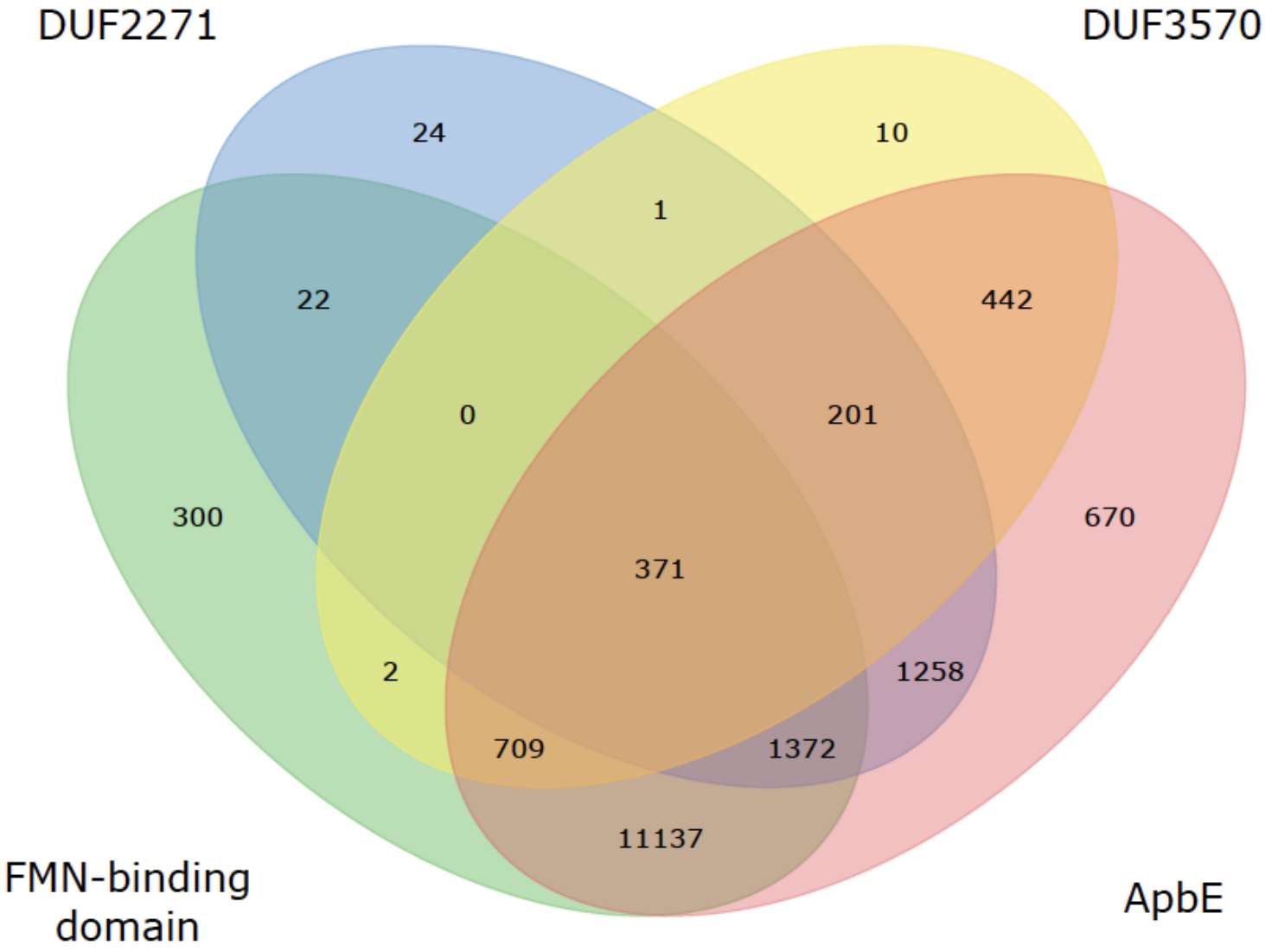

Supplementary Figure 3. Presence of *apbE* and its putative substrates in prokaryotic genomes. Venn diagram showing numbers of shared protein-coding genes between the genomes. Only genomes with a signal peptide predicted in at least one of the four genes are included.

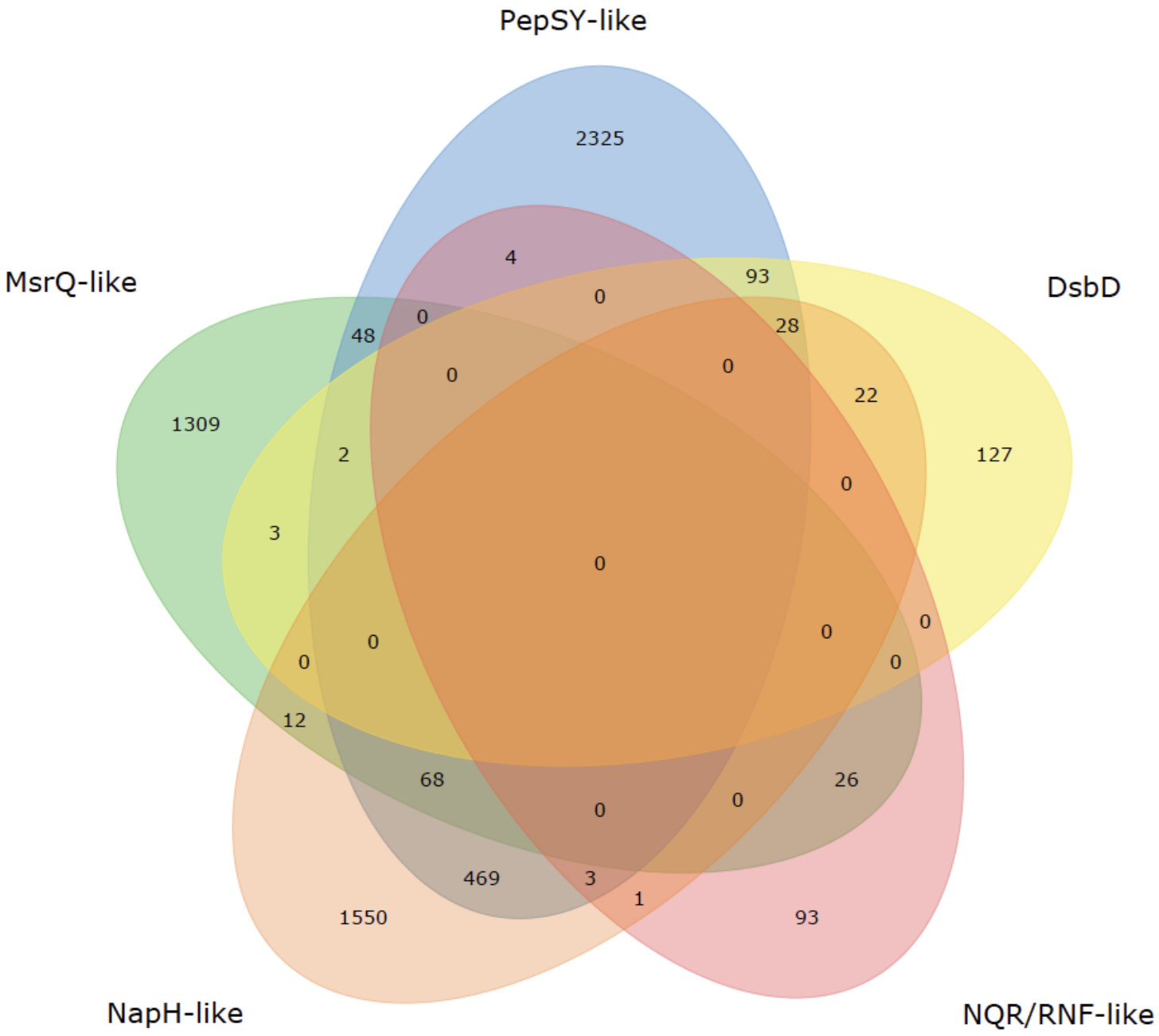

Supplementary Figure 4. Distribution of uncharacterized extracytosolic electron transfer systems within prokaryotic genomes. Venn diagram showing the number of uncharacterized systems (summarized in **Figure 4**) within the 6,366 genomes that have at least one of the uncharacterized extracytosolic electron transfer systems.

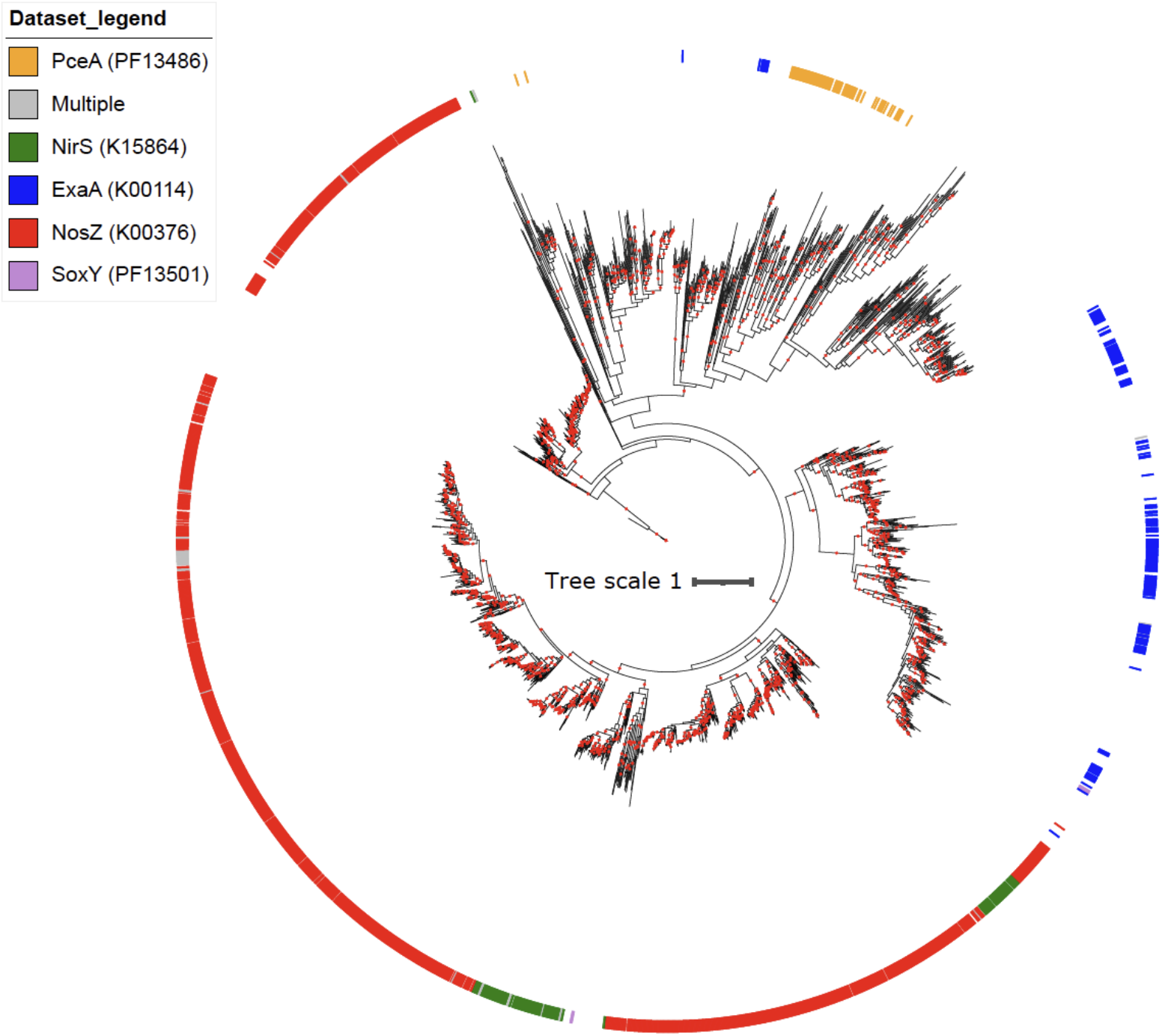

Supplementary Figure 5. Maximum likelihood phylogeny of flavinylation-associated NapH-like proteins. Flavinylation-associated NapH-like proteins… The tree was inferred using an LG+F+I+G4 model of evolution. Scale bar indicates the mean number of substitutions per site. Branches with bootstrap values ≥95 are indicated by red circles. The outer ring indicates the genes associated with the gene clusters.

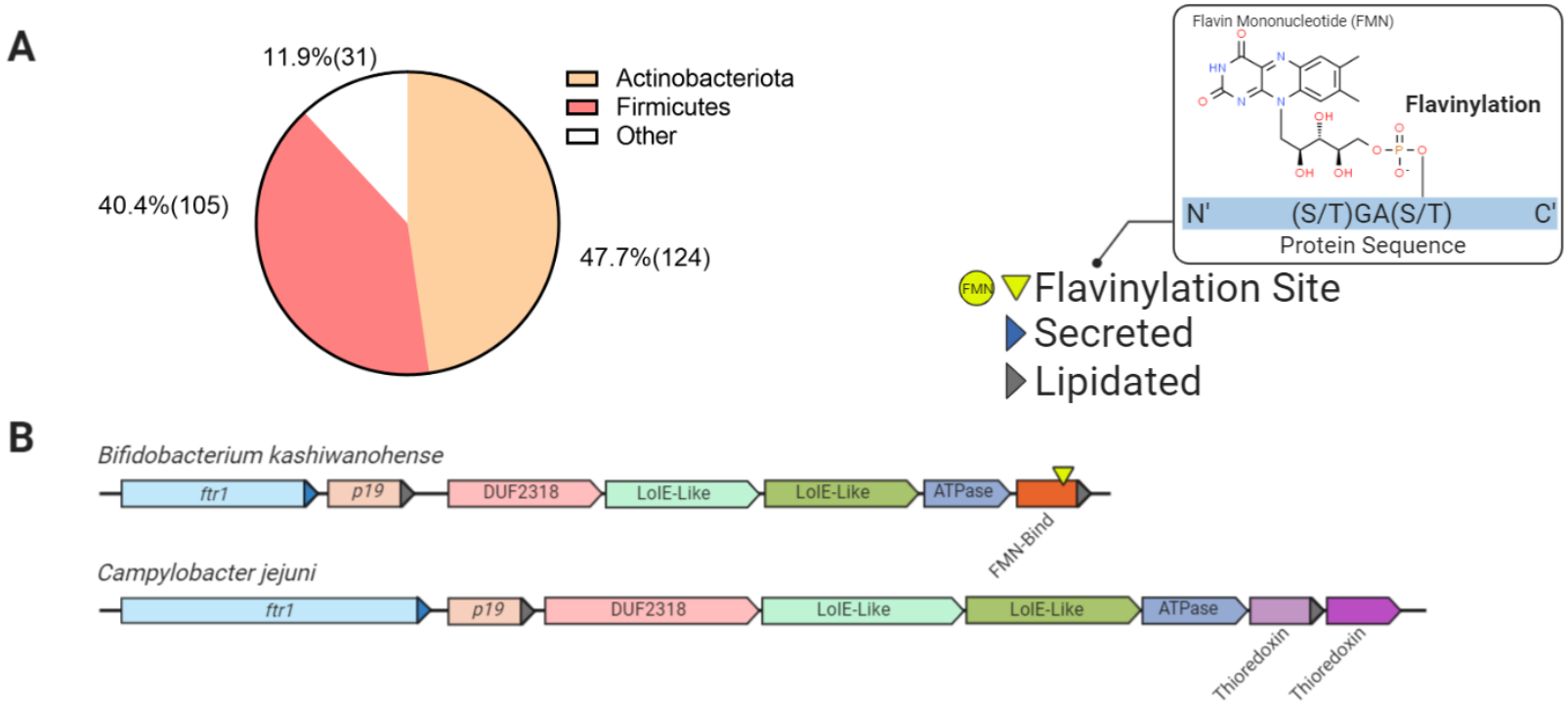

Supplementary Figure 6. Representative P19 gene clusters. (A) Pie chart showing the number of genomes within each phylum with a P19-containing flavinylation-associated gene cluster. (B) Representative P19 gene clusters with thioredoxin-like or FMN-binding proteins. The *Campylobacter jejuni* cluster includes a mechanistically uncharacterized iron transporter and a thioredoxin-like protein [33]. P19 clusters in other genomes, such as *Bifidobacterium kashiwanohense*, lack the thioredoxin-like gene, but contain a gene with an FMN-binding domain.

System	Feature within flavinylation-associated gene clusters used to operationally define system	Number of gene clusters	Number of genomes
EET	Ndh with a transmembrane helix (K03885)	553	547
RNF	RnfB (K03616)	5482	5401
NQR	NqrF (K00351)	3990	3935
Nos	Nitrous-oxide reductase (K00376)	1209	1187
PepSY-like	PepSY-like domain (PF03929 or PF16357)	3220	3040
DsbD-like	DsbD-like domain (PF02683)	285	275
NapH-like	Iron-sulfur cluster-binding protein NapH (PF12801 or K19339)	2465	2153
MsrQ-like	MsrQ-like domain (PF01794)	1797	1468
NQR/RNF-like	NqrB/RnfD (PF03116) and NqrF (PF00175) fusion	127	127

Supplementary Table 1. Summary of prevalence of characterized and uncharacterized systems in prokaryotic genomes.

	PF00890 + cytochrome + FMN-bind (FUSED)	PF00890 + cytochrome (FUSED)	PF00890 + FMN-bind (FUSED)	PF00890, cytochrome, FMN-bind (UNFUSED)	PF00890, cytochrome (UNFUSED)	PF00890, FMN-bind (UNFUSED)
Number of gene clusters	0	147	2979	22	879	189
Number of genomes	0	108	1236	22	360	171

Supplementary Table 2. Fumarate reductase-like associations with FMN-binding domains and cytochromes

References

1. Schröder, I., Johnson, E. & de Vries, S. Microbial ferric iron reductases. *FEMS Microbiol. Rev.* **27**, 427–447 (2003).
2. Bertini, I., Cavallaro, G. & Rosato, A. Cytochrome c: occurrence and functions. *Chem. Rev.* **106**, 90–115 (2006).
3. Cho, S. H. & Collet, J. F. Many roles of the bacterial envelope reducing pathways. *Antioxid. Redox Signal.* **18**, 1690–1698 (2013).
4. Collet, J.-F. & Messens, J. Structure, function, and mechanism of thioredoxin proteins. *Antioxid. Redox Signal.* **13**, 1205–1216 (2010).
5. Bertsova, Y. V. *et al.* Alternative pyrimidine biosynthesis protein ApbE is a flavin transferase catalyzing covalent attachment of FMN to a threonine residue in bacterial flavoproteins. *J. Biol. Chem.* **288**, 14276–14286 (2013).
6. Zhou, W. *et al.* Sequencing and preliminary characterization of the Na+-translocating NADH:ubiquinone oxidoreductase from Vibrio harveyi. *Biochemistry* **38**, 16246–16252 (1999).
7. Backiel, J. *et al.* Covalent binding of flavins to RnfG and RnfD in the Rnf complex from Vibrio cholerae. *Biochemistry* **47**, 11273–11284 (2008).
8. Light, S. H. *et al.* A flavin-based extracellular electron transfer mechanism in diverse Gram-positive bacteria. *Nature* **562**, 140–157 (2018).
9. Zhang, L., Trncik, C., Andrade, S. L. A. & Einsle, O. The flavinyl transferase ApbE of Pseudomonas stutzeri matures the NosR protein required for nitrous oxide reduction. *Biochimica et Biophysica Acta - Bioenergetics* **1858**, 95–102 (2017).
10. Buttet, G. F., Willemin, M. S., Hamelin, R., Rupakula, A. & Maillard, J. The membrane-bound C subunit of reductive dehalogenases: Topology analysis and reconstitution of the FMN-binding domain of pceC. *Front. Microbiol.* (2018) doi:10.3389/fmicb.2018.00755.
11. Light, S. H. *et al.* Extracellular electron transfer powers flavinylated extracellular reductases in Gram-positive bacteria. *Proc. Natl. Acad. Sci. U. S. A.* (2019) doi:10.1073/pnas.1915678116.
12. Bogachev, A. V., Bertsova, Y. V., Bloch, D. A. & Verkhovsky, M. I. Urocanate reductase: Identification of a novel anaerobic respiratory pathway in Shewanella oneidensis MR-1. *Mol. Microbiol.* **86**, 1452–1463 (2012).
13. Kees, E. D. *et al.* Secreted flavin cofactors for anaerobic respiration of fumarate and urocanate by Shewanella oneidensis: Cost and role. *Appl. Environ. Microbiol.* **85**, 1–12 (2019).
14. Burstein, D. *et al.* New CRISPR-Cas systems from uncultivated microbes. *Nature* **542**, 237–241 (2017).
15. Crits-Christoph, A., Diamond, S., Butterfield, C. N., Thomas, B. C. & Banfield, J. F. Novel soil bacteria possess diverse genes for secondary metabolite biosynthesis. *Nature* **558**, 440–444 (2018).
16. Doron, S. *et al.* Systematic discovery of antiphage defense systems in the microbial pangenome. *Science* **359**, 0–12 (2018).
17. Aravind, L. Guilt by association: contextual information in genome analysis. *Genome Res.* **10**, 1074–1077 (2000).
18. Parks, D. H. *et al.* A complete domain-to-species taxonomy for Bacteria and Archaea. *Nat. Biotechnol.* **38**, 1079–1086 (2020).
19. Parks, D. H. *et al.* A standardized bacterial taxonomy based on genome phylogeny substantially revises the tree of life. *Nat. Biotechnol.* **36**, 996–1004 (2018).
20. Brondijk, T. H. C., Fiegen, D., Richardson, D. J. & Cole, J. A. Roles of NapF, NapG and NapH, subunits of the Escherichia coli periplasmic nitrate reductase, in ubiquinol oxidation. *Mol. Microbiol.* **44**, 245–255 (2002).
21. Gennaris, A. *et al.* Repairing oxidized proteins in the bacterial envelope using respiratory chain electrons. *Nature* **528**, 409–412 (2015).
22. Zhang, X., Krause, K.-H., Xenarios, I., Soldati, T. & Boeckmann, B. Evolution of the ferric reductase domain (FRD) superfamily: modularity, functional diversification, and signature motifs. *PLoS One* **8**, e58126 (2013).
23. Peng, E. D. & Payne, S. M. Vibrio cholerae VciB mediates iron reduction. *J. Bacteriol.* **199**, 1–18 (2017).
24. Wan, X. F. *et al.* Transcriptomic and proteomic characterization of the Fur modulon in the metal-reducing bacterium Shewanella oneidensis. *J. Bacteriol.* **186**, 8385–8400 (2004).
25. da Silva Neto, J. F., Lourenço, R. F. & Marques, M. V. Global transcriptional response of

Caulobacter crescentus to iron availability. *BMC Genomics* **14**, 549 (2013).
26. Manck, L. E., Espinoza, J. L., Dupont, C. L. & Barbeau, K. A. Transcriptomic Study of Substrate-Specific Transport Mechanisms for Iron and Carbon in the Marine Copiotroph Alteromonas macleodii. *mSystems* **5**, (2020).
27. Liu, L., Li, S., Wang, S., Dong, Z. & Gao, H. Complex iron uptake by the putrebactin- mediated and Feo systems in Shewanella oneidensis. *Appl. Environ. Microbiol.* **84**, 1–17 (2018).
28. Missiakas, D., Schwager, F. & Raina, S. Identification and characterization of a new disulfide isomerase-like protein (DsbD) in Escherichia coli. *EMBO J.* **14**, 3415–3424 (1995).
29. Krupp, R., Chan, C. & Missiakas, D. DsbD-catalyzed Transport of Electrons across the Membrane of Escherichia coli. *J. Biol. Chem.* **276**, 3696–3701 (2001).
30. Juárez, O., Morgan, J. E., Nilges, M. J. & Barquera, B. Energy transducing redox steps of the Na+-pumping NADH:quinone oxidoreductase from Vibrio cholerae. *Proc. Natl. Acad. Sci. U. S. A.* **107**, 12505–12510 (2010).
31. Steuber, J. *et al.* Structure of the V. cholerae Na+-pumping NADH: Quinone oxidoreductase. *Nature* **516**, 62–67 (2014).
32. Chan, A. C. K. *et al.* Structure and function of P19, a high-affinity iron transporter of the human pathogen campylobacter jejuni. *J. Mol. Biol.* **401**, 590–604 (2010).
33. Liu, M. M. *et al.* Investigating the Campylobacter jejuni Transcriptional Response to Host Intestinal Extracts Reveals the Involvement of a Widely Conserved Iron Uptake System. *MBio* **9**, 1–18 (2018).
34. Jardim-Messeder, D. *et al.* Fumarate reductase superfamily: A diverse group of enzymes whose evolution is correlated to the establishment of different metabolic pathways. *Mitochondrion* **34**, 56–66 (2017).
35. Mikoulinskaia, O., Akimenko, V., Galouchko, A., Thauer, R. K. & Hedderich, R. Cytochrome c-dependent methacrylate reductase from Geobacter sulfurreducens AM-1. *Eur. J. Biochem.* **263**, 346–352 (1999).
36. Schobert, M. & Görisch, H. Cytochrome c550 is an essential component of the quinoprotein ethanol oxidation system in Pseudomonas aeruginosa: Cloning and sequencing of the genes encoding cytochrome c550 and an adjacent acetaldehyde dehydrogenase. *Microbiology* **145**, 471–481 (1999).
37. DiChristina, T. J. & DeLong, E. F. Isolation of anaerobic respiratory mutants of Shewannella putrefaciens and genetic analysis of mutants deficient in anaerobic growth on Fe3+. *J. Bacteriol.* **176**, 1468–1474 (1994).
38. Blumberger, J. Electron transfer and transport through multi-heme proteins: recent progress and future directions. *Curr. Opin. Chem. Biol.* **47**, 24–31 (2018).
39. Wang, F. *et al.* Structure of Microbial Nanowires Reveals Stacked Hemes that Transport Electrons over Micrometers. *Cell* **177**, 361–369.e10 (2019).
40. El-Naggar, M. Y. *et al.* Electrical transport along bacterial nanowires from Shewanella oneidensis MR-1. *Proceedings of the National Academy of Sciences* **107**, 18127–18131 (2010).
41. Holmes, D. E. *et al.* A Membrane-Bound Cytochrome Enables Methanosarcina acetivorans To Conserve Energy from Extracellular Electron Transfer. *mBio* vol. 10 (2019).
42. Yoch, D. C. & Valentine, R. C. Ferredoxins and flavodoxins of bacteria. *Annu. Rev. Microbiol.* **26**, 139–162 (1972).
43. Smillie, R. M. Isolation of two proteins with chloroplast ferredoxin activity from a blue-green alga. *Biochem. Biophys. Res. Commun.* **20**, 621–629 (1965).
44. Knight, E., Jr, D'Eustachio, A. J. & Hardy, R. W. Flavodoxin: a flavoprotein with ferredoxin activity from Clostrium pasteurianum. *Biochim. Biophys. Acta* **113**, 626–628 (1966).
45. Liu, X. *et al.* Power generation from ambient humidity using protein nanowires. *Nature* **578**, 550–554 (2020).
46. Palfey, B. A. & Massey, V. Flavin-dependent enzymes. *Comprehensive biological catalysis* **3**, 83–154 (1998).
47. Eddy, S. R. Profile hidden Markov models. *Bioinformatics* vol. 14 755–763 (1998).
48. Aramaki, T. *et al.* KofamKOALA: KEGG Ortholog assignment based on profile HMM and adaptive score threshold. *Bioinformatics* **36**, 2251–2252 (2020).
49. Mistry, J. *et al.* Pfam: The protein families database in 2021. *Nucleic Acids Res.* (2020) doi:10.1093/nar/gkaa913.
50. Almagro Armenteros, J. J. *et al.* SignalP 5.0 improves signal peptide predictions using deep neural networks. *Nat. Biotechnol.* **37**, 420–423 (2019).

51. Krogh, A., Larsson, B., von Heijne, G. & Sonnhammer, E. L. L. Predicting transmembrane protein topology with a hidden markov model: application to complete genomes11Edited by F. Cohen. *Journal of Molecular Biology* vol. 305 567–580 (2001).
52. Katoh, K. & Standley, D. M. A simple method to control over-alignment in the MAFFT multiple sequence alignment program. *Bioinformatics* **32**, 1933–1942 (2016).
53. Capella-Gutiérrez, S., Silla-Martínez, J. M. & Gabaldón, T. trimAl: a tool for automated alignment trimming in large-scale phylogenetic analyses. *Bioinformatics* **25**, 1972–1973 (2009).
54. Nguyen, L.-T., Schmidt, H. A., von Haeseler, A. & Minh, B. Q. IQ-TREE: A Fast and Effective Stochastic Algorithm for Estimating Maximum-Likelihood Phylogenies. *Mol. Biol. Evol.* **32**, 268–274 (2014).
55. Kalyaanamoorthy, S., Minh, B. Q., Wong, T. K. F., von Haeseler, A. & Jermiin, L. S. ModelFinder: fast model selection for accurate phylogenetic estimates. *Nat. Methods* **14**, 587–589 (2017).
56. Hoang, D. T., Chernomor, O., von Haeseler, A., Minh, B. Q. & Vinh, L. S. UFBoot2: Improving the Ultrafast Bootstrap Approximation. *Molecular Biology and Evolution* vol. 35 518–522 (2018).
57. Madeira, F. *et al.* The EMBL-EBI search and sequence analysis tools APIs in 2019. *Nucleic Acids Res.* **47**, W636–W641 (2019).
58. Wagih, O. ggseqlogo: a versatile R package for drawing sequence logos. *Bioinformatics* **33**, 3645–3647 (2017).